

Homo- and Heterovalent Substitutions in the New Clathrates I $\text{Si}_{30}\text{P}_{16}\text{Te}_{8-x}\text{Se}_x$ and $\text{Si}_{30+x}\text{P}_{16-x}\text{Te}_{8-x}\text{Br}_x$: Synthesis, Crystal Structure, and Thermoelectric Properties

Nikolay S. Abramchuk,^{*,†} Wilder Carrillo-Cabrera,[†] Igor Veremchuk,[†] Niels Oeschler,[†] Andrei V. Olenov,^{‡,||} Yurii Prots,[†] Ulrich Burkhardt,[†] Evgeny V. Dikarev,[§] Juri Grin,[†] and Andrei V. Shevelkov^{*,‡}

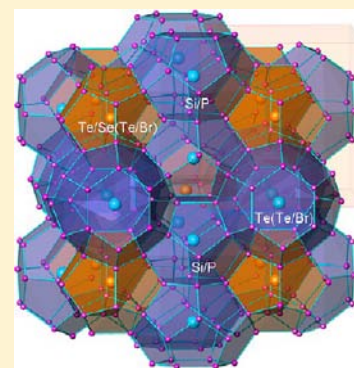
[†]Max-Planck-Institute für Chemische Physik fester Stoffe, Noethnitzer Str. 40, 01187 Dresden, Germany

[‡]Chemistry Department, Lomonosov Moscow State University, Leninskie Gory 1-3, 119991 Moscow, Russia

[§]Department of Chemistry, State University of New York at Albany, Albany, New York 12222, United States

S Supporting Information

ABSTRACT: The new cationic clathrates I $\text{Si}_{30}\text{P}_{16}\text{Te}_{8-x}\text{Se}_x$ and $\text{Si}_{30+x}\text{P}_{16-x}\text{Te}_{8-x}\text{Br}_x$ were synthesized by the standard ampule technique. The $\text{Si}_{30}\text{P}_{16}\text{Te}_{8-x}\text{Se}_x$ ($x = 0-2.3$) clathrates crystallize in the cubic space group $Pm\bar{3}n$ with the unit cell parameter a ranging from 9.9382(2) to 9.9696(1) Å. In the case of the $\text{Si}_{30+x}\text{P}_{16-x}\text{Te}_{8-x}\text{Br}_x$ ($x = 1-6.4$) clathrates, the lattice parameter varies from 9.9720(8) to 10.0405(1) Å; at lower Si/P ratios ($x = 1-3$) the ordering of bromine atoms induces the splitting of the guest positions and causes the transformation from the space group $Pm\bar{3}n$ to $Pm\bar{3}$. Irrespective of the structure peculiarities, the normal temperature motion of the guest atoms inside the oversized cages of the framework is observed. The title clathrates possess very low thermal expansion coefficients ranging from 6.6×10^{-6} to $1.0 \times 10^{-5} \text{ K}^{-1}$ in the temperature range of 298–1100 K. The characteristic Debye temperature is about 490 K. Measurements of the electrical resistivity and thermopower showed typical behavior of p -type thermally activated semiconductors, whereas the temperature behavior of the thermal conductivity is glasslike and in general consistent with the PGEC concept. The highest value of the thermoelectric figure of merit ($ZT = 0.1$) was achieved for the Br-bearing clathrate $\text{Si}_{32.1(2)}\text{P}_{13.9(2)}\text{Te}_{6.6(2)}\text{Br}_{1.0(1)}$ at 750 K.



■ INTRODUCTION

Clathrates are compounds with a covalently bonded framework (host), whose cavities are occupied by atoms, molecules, or ions (guest). The host framework and guest ions of the cationic and anionic clathrates are oppositely charged. The first anionic (intermetallic) clathrates $\text{Na}_8\text{Si}_{46}$ and $\text{Na}_x\text{Si}_{136}$ were synthesized in 1963.^{1,2} $\text{Na}_8\text{Si}_{46}$ crystallizes in the cubic space group $Pm\bar{3}n$ with 46 silicon atoms (host) distributed over 3 positions: $6c$, $16i$, and $24k$, thus forming two types of cages in the framework: pentagonal dodecahedral (20 vertex) and tetrakaidecahedral (24 vertex). Sodium cations (guest) occupy positions in the centers of the pentagonal dodecahedra (site $2a$) and tetrakaidecahedra (site $6d$). There are numerous anionic clathrates, in which the host framework is formed by the elements of groups 13–15 (B, Si, Al, Ge, Sn, In, Ga, and P) and sometimes also include Pd, Pt, Cu, or Ag, while the guest atoms are represented by Na, K, Rb, Cs, Sr, Ba, Eu,^{3–17} etc.

In contrast to the anionic type I clathrates, there is a series of clathrates with inverse host–guest polarity. This group of compounds is called cationic (inverse) clathrates. The first representatives ($\text{Ge}_{38}\text{A}_8\text{X}_8$; $\text{A} = \text{P, As, Sb}$; $\text{X} = \text{Cl, Br, I}$) were prepared by Menke and von Schnering.^{18–20} Recently several cationic clathrates with Sn, Ge, Si, Zn, Cu, P, or As forming the

frameworks and halogenide or chalcogenide ions as guests were described.^{21–35}

A large number of cationic clathrates (in particular of germanium and tin as a main framework component) can be rationalized within the Zintl concept. They display physical properties of narrow-band semiconductors or bad metals.³⁶ The recent significant interest in clathrate compounds is caused by their perspective as thermoelectric materials.³⁷ From this point of view, the recently described cationic clathrates I of the ternary Si–P–Te system^{29–32} are the most interesting, as they combine high thermal and chemical stability with the promising values of the thermoelectric figure of merit.³⁵

In this paper we present the synthesis, crystal structure, and thermoelectric properties of the new quaternary clathrate I phases $\text{Si}_{30}\text{P}_{16}\text{Te}_{8-x}\text{Se}_x$ and $\text{Si}_{30+x}\text{P}_{16-x}\text{Te}_{8-x}\text{Br}_x$. The main task of this work is to determine the influence of substitution of Te by the homovalent Se and heterovalent Br guests on the structural peculiarities and thermoelectric properties.

Received: May 15, 2012

Published: October 16, 2012

EXPERIMENTAL SECTION

Sample Preparation. Silicon (Si, Chempur, 99.999%), red phosphorus (P, 99.999%, Alfa Aesar), tellurium (Te, 99.999%, Chempur), selenium (Se, 99.999%, Chempur), and tellurium bromide (TeBr_4 , 99.9%, Alfa Aesar) were used as the starting components for the synthesis of new cationic clathrates. Pieces of silicon, tellurium, and selenium granules were sequentially ground first in a tungsten carbide (WC) mortar and then in an agate mortar. Pieces of phosphorus were crushed in an agate mortar. For preparation of $\text{Si}_{30}\text{P}_{16}\text{Te}_{8-x}\text{Se}_x$ and $\text{Si}_{30+x}\text{P}_{16-x}\text{Te}_{8-x}\text{Br}_x$ the stoichiometric mixtures of the starting compounds (total weight 0.7–1.0 g) were placed in quartz ampules (outer diameter 14 mm, inner diameter 10 mm, length 60–70 mm), sealed under vacuum ($P \approx 0.01$ – 0.1 Pa), and then transferred into a furnace. In the case of $\text{Si}_{30}\text{P}_{16}\text{Te}_{8-x}\text{Se}_x$, the samples were heated over 24–30 h to 1373 K and kept for 24 h at this temperature, slowly cooled to 1173 K, annealed for 96 h, and finally cooled to room temperature with the furnace. In the case of $\text{Si}_{30+x}\text{P}_{16-x}\text{Te}_{8-x}\text{Br}_x$, the annealing was performed at 1373 K over 168 h. The gray polycrystalline products (particle size up to 1.5 mm) displayed a metallic luster. Preparation and handling of the samples were carried out in an argon-filled glovebox (content of $\text{O}_2 < 1$ ppm, $\text{H}_2\text{O} < 1$ ppm).

In order to obtain bulk samples suitable for physical measurements, spark plasma sintering (SPS)³⁸ was applied (SPS-515 ET/M apparatus, Synthex Ltd., Tokyo). The prepared products (see above), total weight 0.6–0.8 g, were ground in an Ar-filled glovebox and loaded into graphite dies of inner diameter 8 mm. Carbon foil was used to separate the powder specimen from the graphite die and punches during the SPS experiments. Densification was performed by heating to 1073 K at 20 K/min under a pressure of 110 MPa under vacuum (< 10 Pa), remaining at this temperature for 2 h, and then cooling to room temperature. The quality and purity of SPS compacted samples were controlled by means of XRD and metallographic investigations. The results of XRD measurements proved that the samples did not change during the SPS process (Figure S1, Supporting Information).

X-ray Powder Diffraction. X-ray powder diffraction data were collected in a transmission mode using a Huber G670 Image Plate Camera, $\text{Cu K}\alpha_1$ radiation ($\lambda = 1.540598$ Å) and a germanium (111) monochromator. Lattice parameters were calculated by least-squares refinement using LaB_6 (cubic, $a = 4.15692$ Å) as an internal standard and the program package WINXPOW.³⁹

The investigation of the temperature expansion of $\text{Si}_{30}\text{P}_{16}\text{Te}_{8-x}\text{Se}_x$ ($x = 1.5$) and $\text{Si}_{30+x}\text{P}_{16-x}\text{Te}_{8-x}\text{Br}_x$ ($x = 2$) clathrates in the range of 298–1073 K was performed by means of X-ray synchrotron powder diffraction at the beamline B2 in HASYLAB at DESY (Hamburg, Germany).⁴⁰ Diffraction experiments were performed using the Debye–Scherrer geometry equipped with the on-site readable image plate detector OBI.⁴¹ The reflection lines of the standard LaB_6 were used to determine the wavelength $\lambda = 0.53835$ Å (Si(111) monochromator). Quartz capillaries (diameter 0.3 mm) were filled with powdered samples under an Ar atmosphere, sealed, and mounted inside a STOE furnace equipped with a EURO THERM temperature controller. Diffraction patterns were collected with the temperature step of 100 K. Lattice parameters were calculated by least-squares refinement using the WinCSD program package.⁴²

Single-Crystal X-ray Diffraction. Single-crystal diffraction data were collected on a Rigaku AFC7 diffractometer equipped with a Mercury CCD detector and CAD-4 (Nonius) diffractometer applying $\text{Mo K}\alpha$ radiation ($\lambda = 0.71073$ Å). The structure refinement was performed using the SHELXL-97 program package.⁴³

The low-temperature single-crystal X-ray diffraction experiments were performed at eight different temperatures between 90 and 293 K on a Bruker SMART APEX CCD-based X-ray diffractometer ($\text{Mo K}\alpha$, $\lambda = 0.71073$ Å) equipped with a Bruker KRYO-FLEX low-temperature attachment. Crystals were mounted on a goniometer head with silicon grease. For each diffraction experiment 1850 frames were collected with a scan step $\Delta\omega = 0.3^\circ$ and an exposure time of 20 s/frame. The experimental intensities were integrated with the Bruker SAINT software package using a narrow-frame integration algorithm

for a cubic unit cell to a maximum 2θ angle of 56.56° ($d = 0.75$ Å resolution). Finally, the cell parameters were refined on the base of analysis of the XYZ centroids of several thousand reflections above $20\sigma(I)$. Experimental data were corrected for absorption effects using the software SADABS.⁴⁴

Thermal Analysis. Differential scanning calorimetry (DSC) and thermal analysis (DTA) were performed with Netzsch DSC 409C and Netzsch STA 449C instruments, respectively, in the temperature range of 300–1373 K with a heating rate of 10 K/min. The samples (20–150 mg) were placed in special quartz crucibles and sealed under vacuum.

Scanning Electron Microscopy. The crystal morphology of the synthesized clathrates was studied by scanning electron microscopy (SEM). SEM investigations were performed by means of an ESEM FEI Quanta 200 FEGi system (FEI Co., Eindhoven, The Netherlands) operated in a high-vacuum mode and at an acceleration voltage of 25 kV.

Metallography and Wavelength Dispersive X-ray Spectroscopy (WDXS). The samples obtained after the SPS treatment were used for metallographic investigations. Pieces of the bulk material were embedded in conductive resin and polished sequentially by SiC abrasive paper (abrasive grit 1200, 2400, and 4000) and a diamond polishing belt (particle size 0.25 μm) using dried hexane as a lubricant under inert conditions in an argon glovebox. The homogeneity of the samples was examined by optical microscopy (Zeiss Axioplan2) in bright-field and polarized light and by material contrast images recorded by the electron probe micro analyzer Cameca SX100 with tungsten cathode using a backscattered electron (BSE) detector.

The composition of the new clathrates was determined by WDXS carried out by means of the electron probe micro analyzer Cameca SX100. The intensities of the X-ray lines $\text{Se K}\alpha$, $\text{P K}\alpha$, $\text{Si K}\alpha$, and $\text{Te L}\alpha$ were determined with focusing monochromator crystals of LiF (lithium fluoride), TAP (thallium acid phthalate) and PET (pentaerythritol). An electron beam 16 nA/15 kV was adjusted for $\text{P K}\alpha$, $\text{Si K}\alpha$ and $\text{Te L}\alpha$ lines. For the excitation of the $\text{Se K}\alpha$ line an electron beam 60 nA/30 kV was used. The signals were compared to the intensities of the reference materials ZrAsSe , SiP_2 , and Te . The content of the four elements was calculated from the measured X-ray intensities applying the $\varphi(\rho z)$ -matrix correction model. The individual accuracies were $(\Delta c)/c \approx 2\%$ (c = concentration in mass %). The bromine content was calculated from the analytical residues.

Physical Property Measurements. Measurements of physical properties were performed on bulk samples $\text{Si}_{30}\text{P}_{16}\text{Te}_{8-x}\text{Se}_x$ ($x = 1.0, 1.5, 2.0$) and $\text{Si}_{30+x}\text{P}_{16-x}\text{Te}_{8-x}\text{Br}_x$ ($x = 2$) prepared by the SPS treatment. For thermal diffusivity measurements the samples were cut into thin disks (diameter 8 mm, thickness ~ 1 mm) which were coated by a thin carbon layer. For measurements of the thermopower and resistivity, rods ($\sim 1.5 \times 1.5 \times 6.0$ mm) were cut from the bulk samples.

High-temperature measurements of thermal diffusivity were carried out with a Netzsch LFA457 Microflash equipment using the laser flash method. Thermal conductivity (κ) at $T \geq 298$ K was calculated as $\kappa = C_p \alpha d$, where C_p is the specific heat, α is the thermal diffusivity, and d is the density of the sample (calculated using the geometric parameters and mass at room temperature). Measurements of the thermopower and resistivity were carried out by means of a ZEM-3 apparatus (ULVAC-RIKO) under a low-pressure helium atmosphere. The thermopower was determined by a static differential method. The resistivity was simultaneously measured by a four-point setup. High-temperature measurements of specific heat were performed using the DSC method in the temperature range of 323–773 K with a heating rate of 20 K/min under an argon atmosphere with the Netzsch STA 449C equipment. Al_2O_3 was used as a standard.

Low-temperature investigations of the thermoelectric properties of $\text{Si}_{30}\text{P}_{16}\text{Te}_{8-x}\text{Se}_x$ ($x = 1.5$) and $\text{Si}_{30+x}\text{P}_{16-x}\text{Te}_{8-x}\text{Br}_x$ ($x = 2$) were carried out in the temperature range of 2–350 K by means of PPMS equipment (Quantum Design). This equipment allows simultaneous measurements of thermal conductivity, electrical resistivity, and thermopower. The specific heat at low temperature was measured

by a relaxation technique in a Physical Property Measurement System (PPMS, Quantum Design) using samples with a mass of 24–35 mg.

RESULTS AND DISCUSSION

Synthesis and Homogeneity Range. $\text{Si}_{30}\text{P}_{16}\text{Te}_{8-x}\text{Se}_x$ The quaternary samples with the general composition $\text{Si}_{30}\text{P}_{16}\text{Te}_{8-x}\text{Se}_x$ were prepared with x ranging from 0 to 2.5. X-ray powder diffraction patterns showed that the clathrate I phase (space group $Pm\bar{3}n$) was formed for Se content up to $x = 2.3$. The samples $\text{Si}_{30}\text{P}_{16}\text{Te}_{6.3}\text{Se}_{1.7}$, $\text{Si}_{30}\text{P}_{16}\text{Te}_6\text{Se}_2$ and $\text{Si}_{30}\text{P}_{16}\text{Te}_{5.7}\text{Se}_{2.3}$ contained only traces of SiP and Si (less than 1 mass %). After annealing the Se-rich sample ($x = 2.5$) contained, apart from the clathrate I phase, also significant amounts of Si together with an unidentified phase. The dependence of the cubic lattice parameter of the $\text{Si}_{30}\text{P}_{16}\text{Te}_{8-x}\text{Se}_x$ solid solution on the starting Se content (x) is illustrated in Figure 1. The lattice parameter decreases with

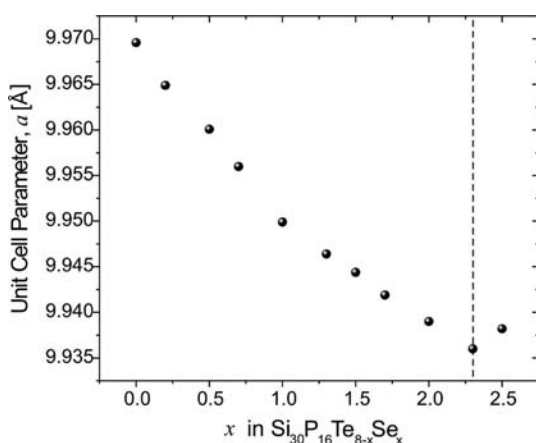


Figure 1. Dependence of the unit cell parameter (a) upon the Se content (x) in $\text{Si}_{30}\text{P}_{16}\text{Te}_{8-x}\text{Se}_x$.

increasing Se content from 9.9696(1) to 9.9382(2) Å. These values are significantly smaller than the lattice parameters reported for $\text{Si}_{46-x}\text{P}_x\text{Te}_y$ ($6.6(1) \leq y \leq 7.5(1)$, $x = 2y$)²⁹ (9.9724(2)–9.9789(2) Å). We conclude that the upper concentration limit of the $\text{Si}_{30}\text{P}_{16}\text{Te}_{8-x}\text{Se}_x$ solid solution corresponds to $x = 2.3$.

Furthermore, the results of the metallographic investigations of $\text{Si}_{30}\text{P}_{16}\text{Te}_{8-x}\text{Se}_x$ ($x < 2.3$) confirmed the absence of significant amounts of minority phases (Figure 2, left). The composition of the clathrate phase in the sample with the starting composition $\text{Si}_{30}\text{P}_{16}\text{Te}_{6.0}\text{Se}_{2.0}$ was $\text{Si}_{30.3(2)}\text{P}_{15.6(2)}\text{Te}_{6.17(4)}\text{Se}_{1.88(5)}$ (WDXS).

$\text{Si}_{30+x}\text{P}_{16-x}\text{Te}_{8-x}\text{Br}_x$ Samples with nominal compositions $\text{Si}_{30+x}\text{P}_{16-x}\text{Te}_{8-x}\text{Br}_x$ ($1 \leq x \leq 6.4$) were prepared. The main phase in these samples crystallizes in the clathrate I type. Only traces of Si and SiP were identified (1 mass % in total). In the case of $\text{Si}_{38}\text{P}_8\text{Br}_8$ ($x = 8$) the clathrate I phase was not found at all. The reaction product contained silicon, phosphorus and Br-bearing amorphous phases. The single-phase character of the product with starting composition $x = 2$ was additionally confirmed by means of metallographic investigations (Figure 2, right). WDXS analysis yielded the composition $\text{Si}_{32.1(2)}\text{P}_{13.9(2)}\text{Te}_{6.6(2)}\text{Br}_{1.0(1)}$.

The XRD patterns of $\text{Si}_{30+x}\text{P}_{16-x}\text{Te}_{8-x}\text{Br}_x$ ($1 \leq x \leq 3$) show additional reflections with $l \neq 2n$ in the $[hhl]$ zone, which should be systematically absent in the $Pm\bar{3}n$ space group. These

patterns were indexed in the $Pm\bar{3}$ space group (Figure 3), whereas the XRD patterns of $\text{Si}_{30+x}\text{P}_{16-x}\text{Te}_{8-x}\text{Br}_x$ with $4 \leq x \leq 6.4$ corresponded to the $Pm\bar{3}n$ space group. The lattice parameter of the clathrate phase varies from 9.9720(8) to 10.0405(1) Å for $1 \leq x \leq 6.4$. In contrast to the case for $\text{Si}_{30}\text{P}_{16}\text{Te}_{8-x}\text{Se}_x$ the lattice parameter of $\text{Si}_{30+x}\text{P}_{16-x}\text{Te}_{8-x}\text{Br}_x$ linearly increases with increasing Br content (Figure 4). The expansion of the lattice parameter can be explained by the increase of silicon content in $\text{Si}_{30+x}\text{P}_{16-x}\text{Te}_{8-x}\text{Br}_x$ with increasing Br content. This is in agreement with the larger covalent radius of Si compared to that of P ($r_{\text{cov}}(\text{Si}) = 1.17$ Å, $r_{\text{cov}}(\text{P}) = 1.10$ Å).⁴⁵ Thus, the effect of the substitution of P by Si atoms on the lattice expansion is stronger than the effect of substitution of Te by Br atoms ($r_{\text{ion}}(\text{Br}^-) = 1.96$ Å, $r_{\text{ion}}(\text{Te}^{2-}) = 2.11$ Å),⁴⁵ which would reduce the lattice parameter.

Description of the Crystal Structure. $\text{Si}_{30}\text{P}_{16}\text{Te}_{8-x}\text{Se}_x$ All synthesized $\text{Si}_{30}\text{P}_{16}\text{Te}_{8-x}\text{Se}_x$ samples contained crystals suitable for single-crystal XRD experiments. Figure 5 illustrates the typical morphology of the crystals. The crystal structures I–III with different selenium contents were solved in the space group $Pm\bar{3}n$ (Table 1).

On the first step of the crystal structure refinement, all positions of the host framework (24k, 16i, and 6c) were set as silicon, whereas Se was introduced as occupying the 2a guest position and Te as the guest in the 6d position. The following isotropic refinement showed that the atomic displacement parameters (ADP) for Si in the position 16i were significantly smaller than for the atoms in the 24k and 6c positions, indicating the preferential occupation of the former position by P atoms. Such a model nicely agrees with the earlier described crystal structures of $\text{Si}_{30}\text{P}_{16}\text{Te}_8$ ³¹ and $\text{Ge}_{30}\text{P}_{16}\text{Te}_8$.⁴⁶ For obvious reasons (close values of Si and P scattering factors), it was not possible to distinguish completely the positions of Si and P within the host framework from the XRD data. In contrast, the distribution of Se and Te within the guest positions was refined accurately. It was demonstrated that the Se atoms occupy the positions inside the 20-vertex cages only. Consequently, the lattice parameter of the clathrates decreases with increasing Se content (Table 1).

In order to investigate the behavior of the crystal structure of $\text{Si}_{30}\text{P}_{16}\text{Te}_{8-x}\text{Se}_x$ (structure IV, $[\text{Si}_6\text{P}]_{46}\text{Te}_{6.78(2)}\text{Se}_{1.22(2)}$) at low temperature, a series of X-ray single crystal diffraction experiments were performed in the temperature range of 90–293 K. Within this temperature range the lattice parameter does not change significantly (Table 2; Figure S2, Supporting Information). In addition, no phase transition was detected.

Figure 6 illustrates the temperature dependences of the atomic displacement parameters for atoms in the guest (6d and 2a) and host framework positions (average value of U_{eq} for atoms in all positions: $-6c$, 16i, 24k) of clathrate crystal structure IV. In contrast to the atoms in the host framework positions, the guest atoms reveal larger ADP values and their temperature dependence is characterized by a larger slope (especially for the 6d position). The nonzero U_{eq} at $T = 0$ is usually associated with the so-called temperature-independent static disorder (d^2).⁴⁷ The temperature dependence of the ADPs for clathrates compounds can be used for estimating the Einstein temperature (Θ_{E}) for the guest atoms (“rattler” acting as the localized harmonic oscillator)^{47–52} and Debye temperature for the whole host framework (Θ_{D}).^{23,47–52}

In accordance with the Einstein model the temperature dependence of ADP is expressed as

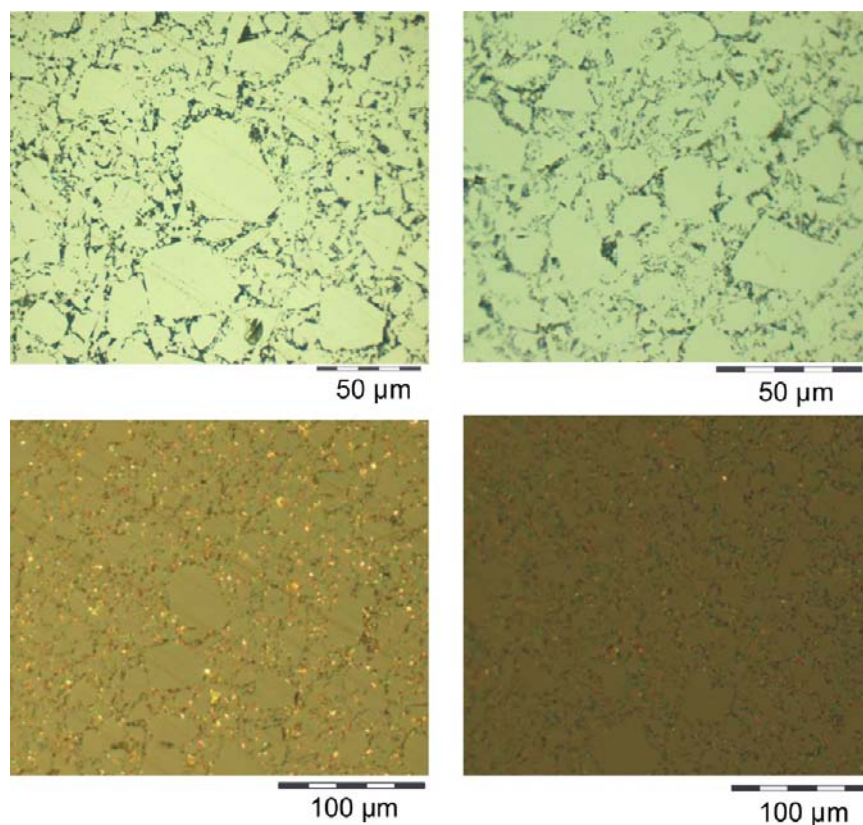


Figure 2. Bright field (top) and polarized light (bottom) images of the bulk (SPS compacted) samples $\text{Si}_{30.3(2)}\text{P}_{15.6(2)}\text{Te}_{6.17(4)}\text{Se}_{1.88(5)}$ (left) and $\text{Si}_{32.1(2)}\text{P}_{13.9(2)}\text{Te}_{6.6(2)}\text{Br}_{1.0(1)}$ (right).

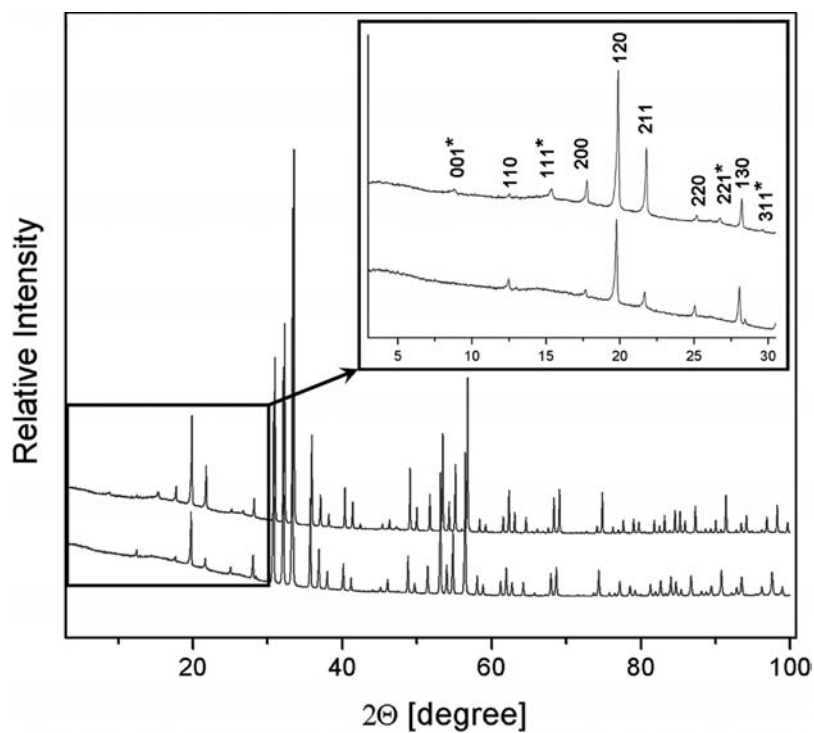


Figure 3. X-ray powder diffraction patterns for $\text{Si}_{30+x}\text{P}_{16-x}\text{Te}_{8-x}\text{Br}_x$ with composition $x = 2$ (top) and $x = 6$ (bottom). The inset shows the representative peaks with $l \neq 2n$ in the $[hhl]$ zone, marked with an asterisk.

$$U_{\text{eq}} = \frac{\hbar^2}{2mk_{\text{B}}\Theta_{\text{E}}} \coth \frac{\Theta_{\text{E}}}{2T} + d^2$$

where U_{eq} is the mean square atomic displacement, m is the atomic mass, \hbar is the Planck constant, and k_{B} is the Boltzmann constant. Using this approach and the results of the fits, we

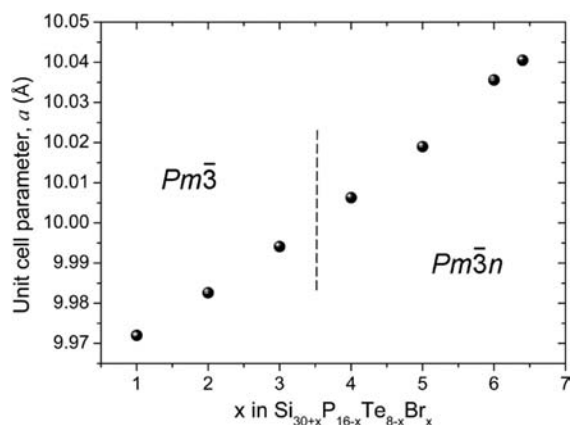


Figure 4. Dependence of the unit cell parameter (a) upon the Br content (x) in $\text{Si}_{30+x}\text{P}_{16-x}\text{Te}_{8-x}\text{Br}_x$.

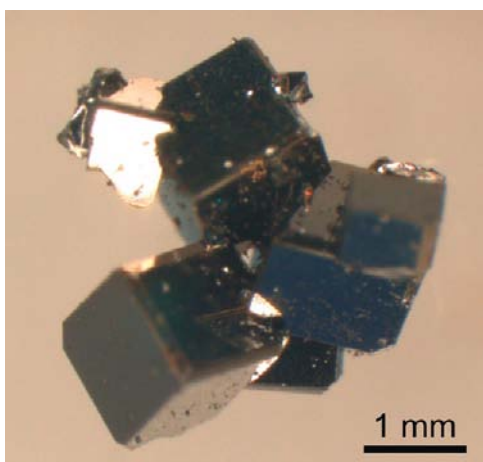


Figure 5. Shape of the single crystals of $\text{Si}_{30}\text{P}_{16}\text{Te}_{8-x}\text{Se}_x$ with $x = 1.5$ (light microscope).

estimated θ_E as 108(1) and 153(1) K with d as 0.085(6) and 0.077(8) Å for the guest atoms in the $6d$ and $2a$ positions, respectively.

The temperature dependence of the ADPs of the host framework atoms were analyzed using the Debye model. For the first approximation, ADPs and atomic mass of the atoms were averaged in accordance with the multiplicity and site occupancy of the positions. Further, the temperature dependence was fitted using the Debye equation:

$$U_{\text{eq}} = \frac{3\hbar^2 T}{mk_B \Theta_D^2} \left[\frac{T}{\Theta_D} \int_0^{\Theta_D/T} \frac{x}{e^x - 1} dx + \frac{\Theta_D}{4T} \right] + d^2$$

In accordance with this approximation, the obtained Debye temperature of the host framework atoms is 491(2) K with $d = 0.045(5)$ Å. This value is significantly higher than that for the clathrates I $\text{Rb}_8\text{Sn}_{44}$ (152(1) K)⁵³ and $\text{Sn}_{24}\text{P}_{19.6(1)}\text{Br}_8$ (220 K)²³ but lower than for the anionic clathrate $\text{Na}_8\text{Si}_{46}$ (570 K).⁵⁴ From the high value of the Debye temperature, we can conclude that the Si-containing clathrate frameworks are rigid irrespective of the nature of the guests and charge distribution.

The calculated value of the Debye temperature was used for estimation of the lattice contribution to the thermal conductivity (κ_l) applying the equation

$$\kappa_l = C_v \nu_s \lambda$$

Table 1. Crystallographic Data for $\text{Si}_x\text{P}_{16}\text{Te}_{8-x}\text{Se}_x$ and $\text{Si}_{30+x}\text{P}_{16-x}\text{Te}_{8-x}\text{Br}_x$

	I	II	III	IV	V	VI
chem formula	$[\text{Si}_x\text{P}_{16}\text{Te}_{6.47(1)}\text{Se}_{1.53(1)}]$	$[\text{Si}_x\text{P}_{16}\text{Te}_{6.74(1)}\text{Se}_{1.26(1)}]$	$[\text{Si}_x\text{P}_{16}\text{Te}_{6.94(2)}\text{Se}_{1.06(2)}]$	$[\text{Si}_x\text{P}_{16}\text{Te}_{6.78(2)}\text{Se}_{1.22(2)}]$	$[\text{Si}_x\text{P}_{16}\text{Te}_{6.0(1)}\text{Br}_{1.5(1)}]$	$[\text{Si}_x\text{P}_{16}\text{Te}_{2.27(7)}\text{Br}_{5.04(8)}]$
space group	$Pm\bar{3}n$	$Pm\bar{3}n$	$Pm\bar{3}n$	$Pm\bar{3}n$	$Pm\bar{3}n$	$Pm\bar{3}n$
a (Å)	9.929(1)	9.938(1)	9.9411(6)	9.955(1)	9.9863(4)	10.0340(4)
V (Å ³)	978.8(1)	981.5(2)	982.4(1)	986.6(1)	995.90(2)	1010.23(7)
Z	1	1	1	1	1	1
T (K)	298	298	298	293	298	298
diffractometer	CAD-4	CAD-4	CAD-4	Bruker SMART APEX	Rigaku AFC7	Rigaku RIG7
λ (Å)	0.710 69	0.710 69	0.710 69	0.710 69	0.710 69	0.710 69
D_{calcd} (g/cm ³)	3.876	3.887	3.900	3.888	3.701	3.310
μ (mm ⁻¹)	7.78	7.70	7.66	7.61	7.42	8.10
$R(F_o)^a$	0.032	0.029	0.021	0.014	0.031	0.023
$R_w(F_o)^b$	0.072	0.049	0.040	0.036	0.083	0.061

^a $R(F_o) = \sum ||F_o| - |F_c|| / \sum |F_o|$. ^b $R_w(F_o^2) = [\sum w(F_o^2 - F_c^2)^2 / \sum w(F_o^2)]^{1/2}$ based on all data.

Table 2. Crystallographic Data for $[\text{Si,P}]_{46}\text{Te}_{6.78(2)}\text{Se}_{1.22(2)}$ at Various Temperatures

T (K)	a (Å)	V (Å ³)	D_{calcd} (g/cm ³)	μ (mm ⁻¹)	$R(F_o)^a$	$R_w(F_o^2)^b$
90	9.958(1)	987.6(2)	3.885	7.60	0.013	0.033
118	9.969(1)	990.79(2)	3.872	7.58	0.014	0.034
143	9.957(1)	987.4(2)	3.886	7.60	0.013	0.033
168	9.958(1)	987.5(1)	3.885	7.60	0.014	0.035
193	9.955(1)	986.5(1)	3.889	7.61	0.013	0.034
218	9.960(1)	988.1(1)	3.883	7.60	0.013	0.034
243	9.972(1)	991.9(1)	3.868	7.57	0.013	0.034
293	9.955(1)	986.6(1)	3.888	7.61	0.014	0.036

^a $R(F_o) = \sum ||F_o| - |F_c|| / \sum |F_o|$. ^b $R_w(F_o^2) = [\sum w(F_o^2 - F_c^2)^2 / \sum w(F_o^2)^2]^{1/2}$ based on all data.

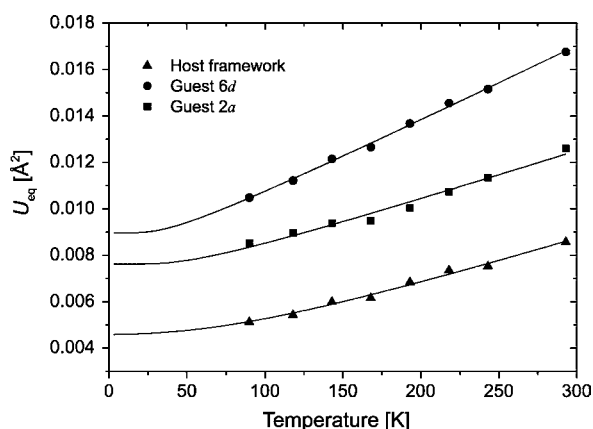


Figure 6. Temperature dependence of the atomic displacement parameters (ADPs) for the atoms in the crystal structure of $[\text{Si,P}]_{46}\text{Te}_{6.78(2)}\text{Se}_{1.22(2)}$. The Einstein temperatures of 108(1) K and 153(1) K for atoms in the 6*d* and 2*a* positions, respectively, and Debye temperature of 491(2) K for host framework atoms were calculated by fitting experimental data.

where v_s is the mean phonon velocity, C_v is the heat capacity per unit volume, and λ is the mean free path of the phonons. In accordance with the Debye model the relation between mean phonon velocity and the Debye temperature is given as $v_s = [(\Theta_D k_B 2\pi) / h] / [6\pi^2(N/V)]^{1/3}$, where N/V is the number of atoms per unit volume. Thus, the calculated v_s for the $[\text{Si,P}]_{46}\text{Te}_{6.78(2)}\text{Se}_{1.22(2)}$ clathrate is about 4352 m/s. Further, the value of the heat capacity was estimated by the Dulong–Petit law $C_v = 3Rn$ (where n is the total number of atoms per formula unit) and is equal to 2.27×10^6 J/(m³ K). Using the same approximation, which was previously described by Kohnir et al.²³ and Kaltzoglou et al.,⁵³ the mean free path of the phonons was estimated as the distance between the Te atoms occupying the 6*d* position and is equal to 4.98×10^{-10} m. On the basis of these data the value of lattice contribution to the thermal conductivity was calculated as 5.0 W/(m K).

$\text{Si}_{30+x}\text{P}_{16-x}\text{Te}_{8-x}\text{Br}_x$. The single-crystal experiments were performed for two specimens with $x = 2$ and $x = 6$ (crystals V and VI, Table 1). The crystal structure V was solved in the space group $Pm\bar{3}$. In the first step of the refinement, all positions of the host framework (12*j*, 12*k*, 8*i*, and 6*f*) were set as completely occupied by Si atoms, whereas the guest positions (6*g*, 1*a*, and 1*b*) were set as mixed occupied by Br and Te atoms. The following refinement showed that the 1*b* position is partially occupied by Br and the 1*a* position contains 55% Te and 45% Br, whereas the 6*g* position is preferred by Te.

Furthermore, the analysis of the ADP's of the host framework atoms and atomic distances allows us to conclude that, as in the case of $\text{Si}_{30}\text{P}_{16}\text{Te}_{8-x}\text{Se}_x$, one of the positions (8*i*) of the host framework is preferentially occupied by P atoms.

The crystal structure VI was solved in the space group $Pm\bar{3}n$. During the refinement, the guest position 6*d* was proved to be occupied by Te and Br atoms, while the position 2*a* was partially occupied by Br. Again, due to the close values of Si and P scattering factors it was not possible to distinguish these atoms in the host framework. Nevertheless, the analysis of the ADPs of atoms and atomic distances allowed us to conclude that the position 16*i* is preferentially occupied by the P atoms.

Therefore, it was demonstrated that partial substitution of Te by Br (at low concentrations) leads to the ordering of bromine atoms in the crystal structure and induces the splitting of the guest positions, which causes the transformation from the space group $Pm\bar{3}n$ to $Pm\bar{3}$ (Scheme S1, Supporting Information).

High-Temperature Structural Behavior. Diffraction experiments performed using X-ray synchrotron radiation revealed that the lattice parameters of $\text{Si}_{30.3(4)}\text{P}_{15.6(3)}\text{Te}_{6.6(1)}\text{Se}_{1.46(9)}$ and $\text{Si}_{32.1(2)}\text{P}_{13.9(2)}\text{Te}_{6.6(2)}\text{Br}_{1.0(1)}$ increase with the temperature (Table 3). Experimental thermal dependences of the unit cell parameter (Figure 7a) were fitted using the phenomenological polynomial function

$$a(T) = a_0(1 + l_1 \times 10^{-6}T + l_2 \times 10^{-9}T^2)$$

Table 3. Lattice Parameters of $\text{Si}_{30.3(4)}\text{P}_{15.6(3)}\text{Te}_{6.6(1)}\text{Se}_{1.46(9)}$ and $\text{Si}_{32.1(2)}\text{P}_{13.9(2)}\text{Te}_{6.6(2)}\text{Br}_{1.0(1)}$ Clathrates Obtained from the High-Temperature Powder Diffraction Data

T (K)	$\text{Si}_{30.3(4)}\text{P}_{15.6(3)}\text{Te}_{6.6(1)}\text{Se}_{1.46(9)}$		$\text{Si}_{32.1(2)}\text{P}_{13.9(2)}\text{Te}_{6.6(2)}\text{Br}_{1.0(1)}$	
	a (Å)	V (Å ³)	a (Å)	V (Å ³)
298	9.9408(1)	982.34(3)	9.9818(4)	994.5(1)
373	9.9453(2)	983.68(6)	9.9873(2)	996.19(6)
473	9.9513(2)	985.46(6)	9.9928(1)	997.83(3)
573	9.9587(2)	987.66(6)	10.0013(2)	1000.39(6)
673	9.9662(2)	989.89(6)	10.0079(1)	1002.37(3)
773	9.9738(2)	992.16(6)	10.0153(2)	1004.60(6)
873	9.9824(2)	994.73(6)	10.0240(2)	1007.22(6)
973	9.9910(2)	997.30(6)	10.0321(2)	1009.66(6)
1073	10.0013(2)	1000.39(6)	10.0413(2)	1012.44(6)

The thermal expansion coefficients were calculated using the derivative approach $\alpha_a = \partial \ln a / \partial T$ ⁵⁵ applied to the data shown in Figure 7a. Figure 7b illustrates that the thermal expansion coefficient for both investigated compositions lies in the range of $(6.0 \times 10^{-6}) - (1.0 \times 10^{-5})$ K⁻¹ for the whole measured temperature range and is even smaller than or comparable to that reported for Si-based clathrates (for example: $\text{Na}_8\text{Si}_{46}$, 2×10^{-5} K⁻¹ at 300 K; $\text{Ba}_8\text{Si}_{46}$, 1.2×10^{-5} K⁻¹ at 300 K; $\text{Ba}_8\text{Pt}_{3.8}\text{Si}_{42.2}$, 6.99×10^{-6} K⁻¹ at 150–300 K; $\text{Ba}_8\text{Ga}_{16}\text{Si}_{30}$, 1.6×10^{-5} K⁻¹ at 300–900 K).⁵⁶

Low-Temperature Thermoelectric Properties. The electrical resistivity and thermopower (Figure 8a,b) show that $\text{Si}_{30.3(4)}\text{P}_{15.6(3)}\text{Te}_{6.6(1)}\text{Se}_{1.46(9)}$ and $\text{Si}_{32.1(2)}\text{P}_{13.9(2)}\text{Te}_{6.6(2)}\text{Br}_{1.0(1)}$ exhibit behavior typical of *p*-type thermally activated semiconductors. The values of the activation energy calculated from the slope of the linear fit of the corresponding dependences of $\ln(1/\rho)$ upon $1/T$ were estimated as $E_g = 0.017$ and 0.020 eV for $\text{Si}_{30.3(4)}\text{P}_{15.6(3)}\text{Te}_{6.6(1)}\text{Se}_{1.46(9)}$ and $\text{Si}_{32.1(2)}\text{P}_{13.9(2)}\text{Te}_{6.6(2)}\text{Br}_{1.0(1)}$, respectively. Therefore, the char-

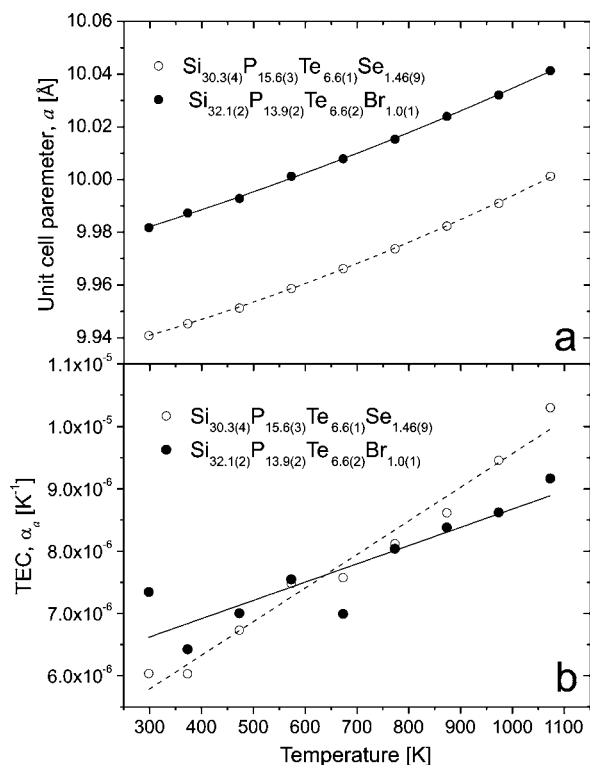


Figure 7. Temperature dependences of the unit cell parameter (a) and the thermal expansion coefficient (b) for $\text{Si}_{30.3(4)}\text{P}_{15.6(3)}\text{Te}_{6.6(1)}\text{Se}_{1.46(9)}$ and $\text{Si}_{32.1(2)}\text{P}_{13.9(2)}\text{Te}_{6.6(2)}\text{Br}_{1.0(1)}$ (the results of least-squares fitting are shown as dashed and solid lines).

acter of the electrical conductivity of $\text{Si}_{30}\text{P}_{16}\text{Te}_{8-x}\text{Se}_x$ and $\text{Si}_{30+x}\text{P}_{16-x}\text{Te}_{8-x}\text{Br}_x$ differs from that of $\text{Si}_{46-x}\text{P}_x\text{Te}_y$, which exhibits the properties of heavily doped semiconductors or semimetals.²⁹ The values of the thermopower for $\text{Si}_{30.3(4)}\text{P}_{15.6(3)}\text{Te}_{6.6(1)}\text{Se}_{1.46(9)}$ and $\text{Si}_{32.1(2)}\text{P}_{13.9(2)}\text{Te}_{6.6(2)}\text{Br}_{1.0(1)}$ clathrates are positive, confirming that holes are the dominant carriers and are close to each other in the whole temperature range. It is interesting to note that the absolute values of the thermopower at low temperatures are close to those reported for Bi_2Te_3 ,⁵⁷ which is the base for the most widely used commercial thermoelectric materials.

The thermal conductivity of $\text{Si}_{30.3(4)}\text{P}_{15.6(3)}\text{Te}_{6.6(1)}\text{Se}_{1.46(9)}$ significantly increases up to approximately 130 K and then becomes constant (Figure 8c). In addition, it should be mentioned that, as is usual for low thermal conductivity materials measured by means of PPMS Quantum Design equipment, the thermal conductivity data show an artificial upturn above 250 K. This is roughly proportional to T^3 and is due to uncorrected radiation heat losses. The temperature dependence of the thermal conductivity for $\text{Si}_{30.3(4)}\text{P}_{15.6(3)}\text{Te}_{6.6(1)}\text{Se}_{1.46(9)}$ is glasslike.⁵⁸ Altogether, the title clathrates display a combination of low thermal conductivity with efficient transport of the charge carriers. According to the phenomenological phonon glass–electron crystal (PGEC)⁵⁹ concept, they should be considered as prospective thermoelectric materials. However, the largest value of the thermoelectric figure of merit (ZT) in the measured temperature range is estimated as 0.022 at 350 K for $\text{Si}_{30.3(4)}\text{P}_{15.6(3)}\text{Te}_{6.6(1)}\text{Se}_{1.46(9)}$.

High-Temperature Thermoelectric Properties. Figure 9 illustrates the temperature dependences of the electrical resistivity, thermopower, thermal conductivity, and thermoelectric figure of merit for the clathrates with the following

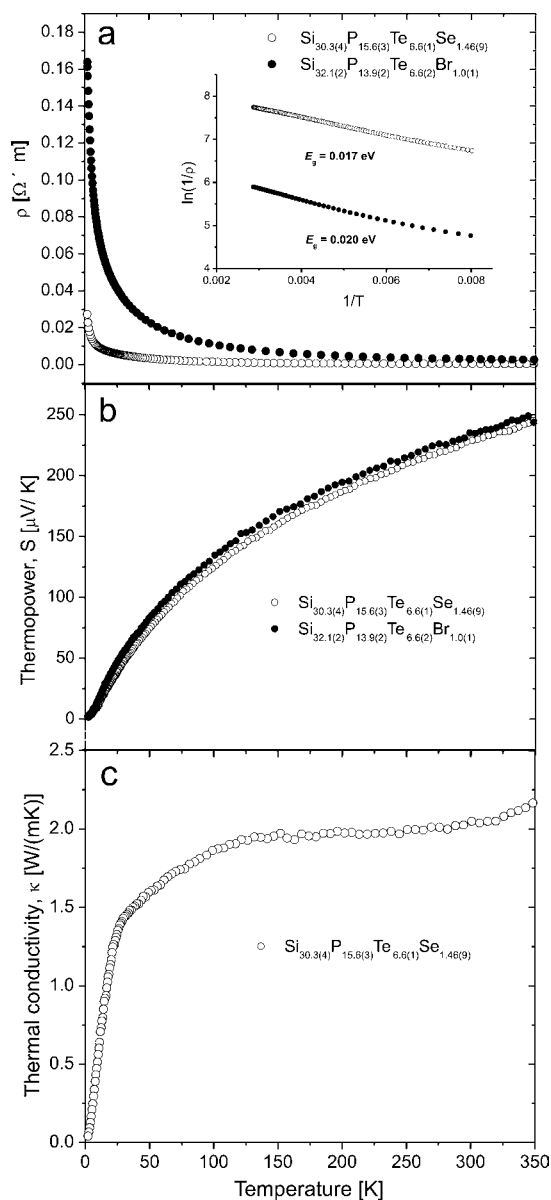


Figure 8. Temperature dependences of the electrical resistivity (a), thermopower (b), and thermal conductivity (c) for $\text{Si}_{30.3(4)}\text{P}_{15.6(3)}\text{Te}_{6.6(1)}\text{Se}_{1.46(9)}$ and $\text{Si}_{32.1(2)}\text{P}_{13.9(2)}\text{Te}_{6.6(2)}\text{Br}_{1.0(1)}$.

compositions: $\text{Si}_{30.3(4)}\text{P}_{15.6(3)}\text{Te}_{6.6(1)}\text{Se}_{1.46(9)}$, $\text{Si}_{29.8(3)}\text{P}_{15.9(2)}\text{Te}_{7.1(1)}\text{Se}_{1.04(3)}$, $\text{Si}_{30.3(2)}\text{P}_{15.6(2)}\text{Te}_{6.17(4)}\text{Se}_{1.88(5)}$, and $\text{Si}_{32.1(2)}\text{P}_{13.9(2)}\text{Te}_{6.6(2)}\text{Br}_{1.0(1)}$. The literature data for clathrate I $\text{Si}_{31.9(1)}\text{P}_{13.9(1)}\text{Te}_{7.00(3)}$ and clathrate III $\text{Si}_{131.8(3)}\text{P}_{40.4(4)}\text{Te}_{21.5(1)}$ ³⁵ are added for comparison.

At high temperature $\text{Si}_{30}\text{P}_{16}\text{Te}_{8-x}\text{Se}_x$ ($x = 1.0, 1.5, \text{ and } 2.0$) and $\text{Si}_{32.1(2)}\text{P}_{13.9(2)}\text{Te}_{6.6(2)}\text{Br}_{1.0(1)}$ clathrates exhibit semiconducting behavior. The electrical resistivity within this temperature range increases with decreasing Se content. For the Br-containing clathrate the electrical resistivity is significantly lower than for all Se-containing ones. On the other hand, the electrical resistivity of $\text{Si}_{30}\text{P}_{16}\text{Te}_{8-x}\text{Se}_x$ is significantly higher than that for the ternary compounds $\text{Si}_{31.9(1)}\text{P}_{13.9(1)}\text{Te}_{7.00(3)}$ (<10 m Ω cm) and $\text{Si}_{131.8(3)}\text{P}_{40.4(4)}\text{Te}_{21.5(1)}$ (<35 m Ω cm) measured in the temperature range 300–800 K.³⁵ In turn, the electrical resistivity of $\text{Si}_{32.1(2)}\text{P}_{13.9(2)}\text{Te}_{6.6(2)}\text{Br}_{1.0(1)}$ is comparable with that of $\text{Si}_{131.8(3)}\text{P}_{40.4(4)}\text{Te}_{21.5(1)}$. It should be noted that $\text{Si}_{30}\text{P}_{16}\text{Te}_{8-x}\text{Se}_x$ and $\text{Si}_{32.1(2)}\text{P}_{13.9(2)}\text{Te}_{6.6(2)}\text{Br}_{1.0(1)}$ are semicon-

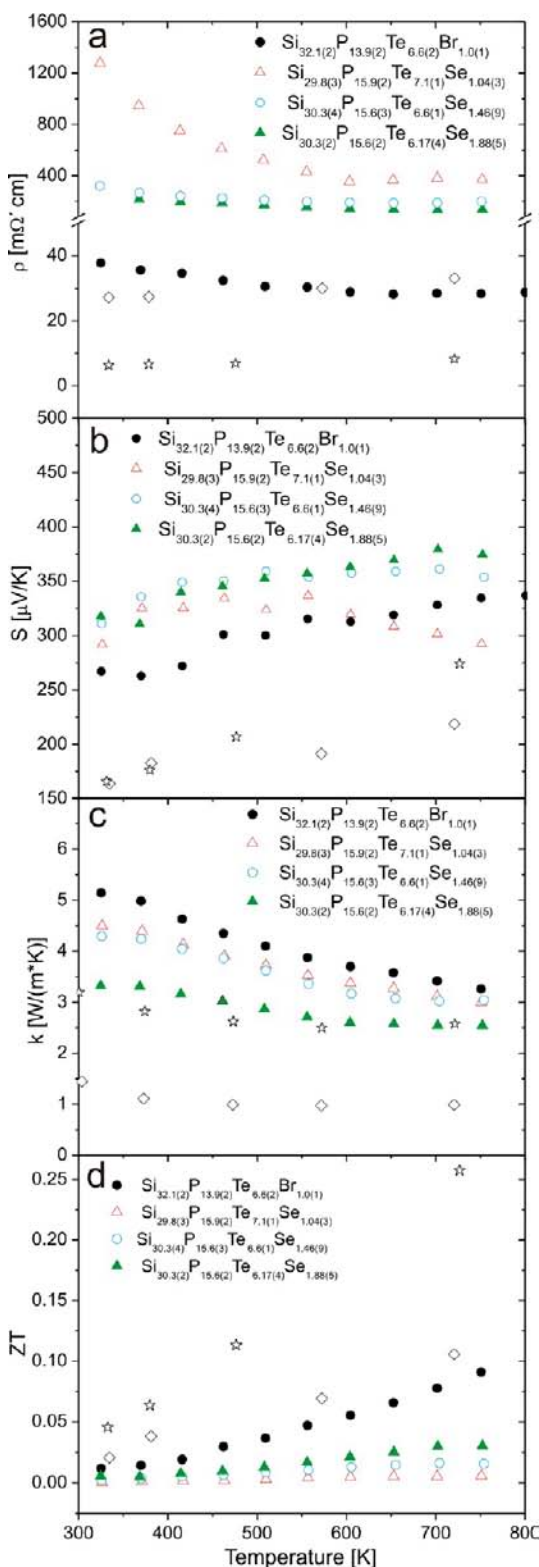


Figure 9. High-temperature dependence of electrical resistivity (a), thermopower (b), thermal conductivity (c), and thermoelectric figure of merit (d) for $\text{Si}_{30}\text{P}_{16}\text{Te}_{8-x}\text{Se}_x$ and $\text{Si}_{32.1(2)}\text{P}_{13.9(2)}\text{Te}_{6.6(2)}\text{Br}_{1.0(1)}$ clathrates. The corresponding values for clathrate I $\text{Si}_{31.9(1)}\text{P}_{13.9(1)}\text{Te}_{7.00(3)}$ and clathrate III $\text{Si}_{131.8(3)}\text{P}_{40.4(4)}\text{Te}_{21.5(1)}$ ³⁵ are shown as open stars and rhombs, respectively.

ductors, whereas $\text{Si}_{31.9(1)}\text{P}_{13.9(1)}\text{Te}_{7.00(3)}$ is a semimetal. As a consequence, for all investigated samples the values of the

thermopower in the temperature range of 300–750 K are higher than for $\text{Si}_{31.9(1)}\text{P}_{13.9(1)}\text{Te}_{7.00(3)}$ and also for $\text{Si}_{131.8(3)}\text{P}_{40.4(4)}\text{Te}_{21.5(1)}$, having a different clathrate-type structure.

In order to estimate the quality of the high-temperature measurements of the specific heat, the results obtained by means of DSC measurements were compared with the corresponding low-temperature data (Figure 10). At temper-

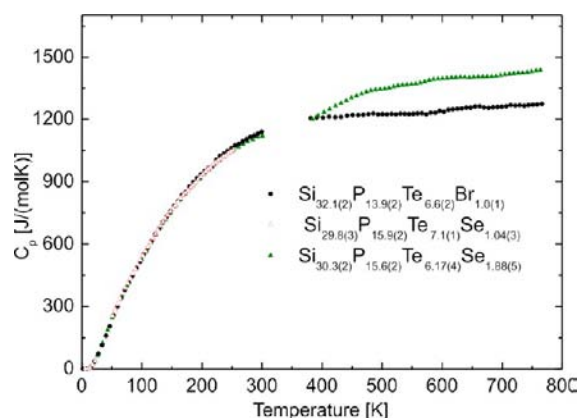


Figure 10. Temperature dependence of the specific heat for $\text{Si}_{30}\text{P}_{16}\text{Te}_{8-x}\text{Se}_x$ and $\text{Si}_{32.1(2)}\text{P}_{13.9(2)}\text{Te}_{6.6(2)}\text{Br}_{1.0(1)}$.

atures higher than the Debye temperature, the values of the heat capacity can be estimated by the Dulong–Petit law. For the clathrates of the Si–P–Te–Se system ($n = 54$) $C_v \approx 1346 \text{ J mol}^{-1} \text{ K}^{-1}$, whereas in the case of $\text{Si}_{32.1(2)}\text{P}_{13.9(2)}\text{Te}_{6.6(2)}\text{Br}_{1.0(1)}$ ($n = 53.5$) C_v is slightly lower, $\sim 1333 \text{ J mole}^{-1} \text{ K}^{-1}$. These values mostly fit the results of the measurements for $\text{Si}_{30.3(2)}\text{P}_{15.6(2)}\text{Te}_{6.17(4)}\text{Se}_{1.88(5)}$ and $\text{Si}_{32.1(2)}\text{P}_{13.9(2)}\text{Te}_{6.6(2)}\text{Br}_{1.0(1)}$. In the case of $\text{Si}_{30.3(4)}\text{P}_{15.6(3)}\text{Te}_{6.6(1)}\text{Se}_{1.46(9)}$ the values of the high-temperature specific heat are significantly higher, while in the case of $\text{Si}_{29.8(3)}\text{P}_{15.9(2)}\text{Te}_{7.1(1)}\text{Se}_{1.04(3)}$ they are significantly lower (not shown in Figure 10). To avoid the data discrepancy, for all compounds of the Si–P–Te–Se system the value of the specific heat for $\text{Si}_{32.1(2)}\text{P}_{13.9(2)}\text{Te}_{6.6(2)}\text{Br}_{1.0(1)}$ was used for the thermal conductivity calculations. The temperature dependence of heat capacity for the selected clathrate (Figure 10) is in the best agreement with the Dulong–Petit law and reaches the saturation value after the Debye temperature.

The thermal conductivity of the investigated clathrates sequentially decreases from $\text{Si}_{32.1(2)}\text{P}_{13.9(2)}\text{Te}_{6.6(2)}\text{Br}_{1.0(1)}$ to $\text{Si}_{30}\text{P}_{16}\text{Te}_{8-x}\text{Se}_x$ and also from $\text{Si}_{29.8(3)}\text{P}_{15.9(2)}\text{Te}_{7.1(1)}\text{Se}_{1.04(3)}$ to $\text{Si}_{30.3(2)}\text{P}_{15.6(2)}\text{Te}_{6.17(4)}\text{Se}_{1.88(5)}$. At the same time, the temperature behavior of the thermal conductivity for the quaternary clathrates is similar to that observed for the clathrates I in the Si–P–Te system,³⁵ whereas the thermal conductivity for the type III clathrate $\text{Si}_{131.8(3)}\text{P}_{40.4(4)}\text{Te}_{21.5(1)}$ is significantly lower. The experimental values of the thermal conductivity at around Debye temperature for Se-containing clathrates is slightly lower (due to the insufficiently high density (around 90% from theoretical value) of SPS compacted samples which were used for the measurements) than the estimated value of the lattice contribution to the thermal conductivity, $\kappa_1 = 5.0 \text{ W/(m K)}$ (see above).

For the $\text{Si}_{30}\text{P}_{16}\text{Te}_{8-x}\text{Se}_x$ clathrates the dimensionless thermoelectric figure of merit $ZT = S^2T/(\kappa\rho)$ reaches a maximum value at around 700 K, whereas it continuously increases for $\text{Si}_{32.1(2)}\text{P}_{13.9(2)}\text{Te}_{6.6(2)}\text{Br}_{1.0(1)}$ in the investigated temperature

range, reaching $ZT = 0.1$ at 750 K (Figure 9d). These values are lower than those for the clathrate I in the Si–P–Te system. However, in the same temperature range, ZT values for the $\text{Si}_{32.1(2)}\text{P}_{13.9(2)}\text{Te}_{6.6(2)}\text{Br}_{1.0(1)}$ are comparable to those of clathrate III in the Si–P–Te system. It can be concluded that for the type I clathrates the mixing of Te/Se (homovalent) or Te/Br (heterovalent) atoms leads to the transition from the semimetallic properties pertinent for $(\text{Si,P})_{46}\text{Te}_{8-y}$ to the properties of typical low-gap p -type semiconductors. In turn, this leads to a lower thermoelectric figure of merit.

CONCLUSIONS

The new cationic (inverse) clathrates I $\text{Si}_{30}\text{P}_{16}\text{Te}_{8-x}\text{Se}_x$ and $\text{Si}_{30+x}\text{P}_{16-x}\text{Te}_{8-x}\text{Br}_x$ were synthesized in the Si–P–Te–Se(Br) systems by the standard ampule technique. All synthesized clathrates crystallize in the cubic system. However, it was demonstrated that for $\text{Si}_{30+x}\text{P}_{16-x}\text{Te}_{8-x}\text{Br}_x$ ($x = 1-6.4$) clathrates with lower Si/P ratio ($x = 1-3$) the ordering of bromine atoms induces the transformation from the space group $Pm\bar{3}n$ to $Pm\bar{3}$. The investigated clathrates are characterized by rigid frameworks and display very low values of the thermal expansion coefficient. Measurements of the electrical resistivity and thermopower showed that the investigated clathrates exhibit behavior typical of p -type thermally activated semiconductors with estimated activation energies of 0.017 and 0.020 eV in the range 2–350 K for $\text{Si}_{30.3(4)}\text{P}_{15.6(3)}\text{Te}_{6.6(1)}\text{Se}_{1.46(9)}$ and $\text{Si}_{32.1(2)}\text{P}_{13.9(2)}\text{Te}_{6.6(2)}\text{Br}_{1.0(1)}$, respectively. Importantly, the character of the electrical conductivity of $\text{Si}_{30}\text{P}_{16}\text{Te}_{8-x}\text{Se}_x$ and $\text{Si}_{30+x}\text{P}_{16-x}\text{Te}_{8-x}\text{Br}_x$ differs from that of the $\text{Si}_{46-x}\text{P}_x\text{Te}_y$ clathrates, which exhibit properties of heavily doped semiconductors or semimetals, depending on their composition. $\text{Si}_{30}\text{P}_{16}\text{Te}_{8-x}\text{Se}_x$ demonstrates glass-like thermal conductivity, hinting at the phonon glass–electron crystal behavior. Altogether, the title clathrates conform to the PGEC concept. The highest value of thermoelectric figure of merit (ZT) was achieved for a Br-bearing clathrate ($\text{Si}_{32.1(2)}\text{P}_{13.9(2)}\text{Te}_{6.6(2)}\text{Br}_{1.0(1)}$) and was estimated as 0.1 (at 750 K). We propose that $\text{Si}_{30}\text{P}_{16}\text{Te}_{8-x}\text{Se}_x$ and $\text{Si}_{30+x}\text{P}_{16-x}\text{Te}_{8-x}\text{Br}_x$ clathrates can be used as a base for the creation of perspective thermoelectric materials for high-temperature applications.

ASSOCIATED CONTENT

Supporting Information

Figures giving an X-ray powder diffraction patterns, a graph of the temperature dependences of the unit cell parameters and atomic displacement parameters, and details of a space group transformation and a CIF file containing information on all structural experiments. This material is available free of charge via the Internet at <http://pubs.acs.org>.

AUTHOR INFORMATION

Corresponding Author

*N.S.A: tel, +4935146462236; fax, +4935146464002; e-mail, Nikolay.Abramchuk@cpfs.mpg.de. A.V.S.: tel, +74959393339; fax, +74959394788; e-mail, shev@inorg.chem.msu.ru.

Present Address

^{||}Department of Chemistry, University of California Davis, One Shields Avenue, Davis, CA 95616.

Author Contributions

The manuscript was written through contributions of all authors. All authors have given approval to the final version of the manuscript.

Notes

The authors declare no competing financial interest.

ACKNOWLEDGMENTS

We thank Dr. S. Hoffmann, Ms. M. Eckert, and Dr. E. V. Rosseeva for the experimental support and Dr. J. V. Zaikina and Prof. Dr. L. Vasylechko for fruitful discussion. A.V.O. and A.V.S. acknowledge the support of the Russian Foundation for Basic Research.

ABBREVIATIONS

PGEC, phonon glass–electron crystal; SPS, spark plasma sintering; CCD, charge-coupled device; HASYLAB, Hamburger Synchrotronstrahlungslabor; DESY, Deutsches Elektronen-Synchrotron; DSC, differential scanning calorimetry; DTA, differential thermal analysis; SEM, scanning electron microscopy; WDXS, wavelength dispersive X-ray spectroscopy; BSE detector, backscattered electron detector; TAP, thallium acid phthalate; PET, pentaerythritol; LFA, laser flash technique; PPMS, Physical Property Measurement System; XRD, X-ray diffraction; ADP, atomic displacement parameters

REFERENCES

- (1) Cros, C.; Hagenmuller, P.; Pouchard, M. *C.R. Seances Acad. Sci. Paris* **1965**, *260* (18), 4764.
- (2) Kasper, J. S.; Hagenmuller, P.; Pouchard, M.; Cros, C. *Science* **1965**, *150* (3704), 1713.
- (3) Jung, W.; Lörrincz, J.; Ramlau, R.; Borrmann, H.; Prots, Yu.; Haarmann, F.; Schnelle, W.; Burkhardt, U.; Baitinger, M.; Grin, Yu. *Angew. Chem., Int. Ed.* **2007**, *46* (35), 6725.
- (4) Condrón, C. L.; Porter, R.; Guo, T.; Kauzlarich, S. M. *Inorg. Chem.* **2005**, *44* (25), 9185.
- (5) Condrón, C. L.; Kauzlarich, S. M.; Nolas, G. S. *Inorg. Chem.* **2007**, *46*, 2556.
- (6) Condrón, C. L.; Martin, J.; Nolas, G. S.; Piccoli, P. M. B.; Schultz, A. J.; Kauzlarich, S. M. *Inorg. Chem.* **2006**, *45* (23), 9381.
- (7) Böhme, B.; Aydemir, U.; Ormeci, A.; Schnelle, W.; Baitinger, M.; Grin, Y. *Sci. Technol. Adv. Mater.* **2007**, *8*, 410.
- (8) Demchyna, R.; Köhler, U.; Prots, Yu.; Schnelle, W.; Baenitz, M.; Burkhardt, U.; Paschen, S.; Schwarz, U. *Z. Anorg. Allg. Chem.* **2006**, *632* (1), 73.
- (9) Böhme, B.; Guloy, A.; Tang, Z.; Schnelle, W.; Burkhardt, U.; Baitinger, M.; Grin, Y. *J. Am. Chem. Soc.* **2007**, *129* (17), 5348.
- (10) Li, Y.; Chi, J.; Gou, W. P.; Khandekar, S.; Ross, J. H. *J. Phys.: Condens. Matter.* **2003**, *15* (32), 5535.
- (11) Johnsen, S.; Bentien, A.; Madsen, G. K. H.; Iversen, B. B.; Nygren, M. *Chem. Mater.* **2006**, *18* (19), 4633.
- (12) Kaltzoglou, A.; Ponou, S.; Fässler, T. F. *Eur. J. Inorg. Chem.* **2008**, *4*, 538.
- (13) Wosylus, A.; Veremchuk, I.; Schnelle, W.; Baitinger, M.; Schwarz, U.; Grin, Yu. *Chem. Eur. J.* **2009**, *15* (24), 5901.
- (14) Kröner, R.; Peters, K.; von Schnering, H. G.; Nesper, R. Z. *Kristallogr.: New Cryst. Struct.* **1998**, *213* (4), 667.
- (15) Kröner, R.; Peters, K.; von Schnering, H. G.; Nesper, R. Z. *Kristallogr.: New Cryst. Struct.* **1998**, *213* (4), 671.
- (16) Cordier, G.; Woll, P. J. *Less-Common Met.* **1991**, *169* (2), 291.
- (17) Dünner, J.; Mewis, A. *Z. Anorg. Allg. Chem.* **1995**, *621* (2), 191.
- (18) Menke, H.; von Schnering, H. G. *Naturwissenschaften* **1972**, *59*, 420.
- (19) Menke, H.; von Schnering, H. G. *Z. Anorg. Allg. Chem.* **1973**, *395*, 223.

- (20) Menke, H.; von Schnering, H. G. *Z. Anorg. Allg. Chem.* **1976**, *424*, 108.
- (21) Shatruck, M. M.; Kovnir, K. A.; Shevelkov, A. V.; Presniakov, I. A.; Popovkin, B. A. *Inorg. Chem.* **1999**, *38* (15), 3455.
- (22) Shatruck, M. M.; Kovnir, K. A.; Lindsjo, M.; Presniakov, I. A.; Kloo, L. A.; Shevelkov, A. V. *J. Solid State Chem.* **2001**, *161* (2), 233.
- (23) Kovnir, K. A.; Zaikina, J. V.; Reshetova, L. N.; Olenev, A. V.; Dikarev, E. V.; Shevelkov, A. V. *Inorg. Chem.* **2004**, *43*, 3230.
- (24) Kovnir, K. A.; Shatruck, M. M.; Reshetova, L. N.; Presniakov, I. A.; Dikarev, E. V.; Baitinger, M.; Haarmann, F.; Schnelle, W.; Baenitz, M.; Grin, Yu.; Shevelkov, A. V. *Solid State Sci.* **2005**, *7*, 957.
- (25) Kovnir, K. A.; Sobolev, A. V.; Presniakov, I. A.; Lebedev, O. I.; Van Tendeloo, G.; Schnelle, W.; Grin, Yu.; Shevelkov, A. V. *Inorg. Chem.* **2005**, *44* (24), 8786.
- (26) Yakimchuk, A. V.; Zaikina, J. V.; Reshetova, L. N.; Ryabova, L. I.; Khokhlov, D. R.; Shevelkov, A. V. *Low Temp. Phys.* **2007**, *33* (2 – 3), 276.
- (27) Zaikina, J. V.; Schnelle, W.; Kovnir, K. A.; Olenev, A. V.; Grin, Yu.; Shevelkov, A. V. *Solid State Sci.* **2007**, *9*, 664.
- (28) Chu, T. L.; Chu, S. S.; Ray, R. L. *J. Appl. Phys.* **1982**, *53*, 7102.
- (29) Zaikina, J. V.; Kovnir, K. A.; Burkhardt, U.; Schnelle, W.; Haarmann, F.; Schwarz, U.; Grin, Yu.; Shevelkov, A. V. *Inorg. Chem.* **2009**, *48* (8), 3720.
- (30) Zaikina, J. V.; Kovnir, K. A.; Schwarz, U.; Borrmann, H.; Shevelkov, A. V. *Z. Kristallogr.: New Cryst. Struct.* **2007**, *222* (3), 177.
- (31) Kishimoto, K.; Koyanagi, T.; Akai, K.; Matsuura, M. *Jpn. J. Appl. Phys.* **2007**, *46* (31), L746.
- (32) Philipp, F.; Schmidt, P. *J. Cryst. Growth* **2008**, *310* (24), 5402.
- (33) Kirsanova, M. A.; Reshetova, L. N.; Olenev, A. V.; Abakumov, A. M.; Shevelkov, A. V. *Chem. Eur. J.* **2011**, *17* (20), 5719.
- (34) Kirsanova, M. A.; Olenev, A. V.; Abakumov, A. M.; Bykov, M. A.; Shevelkov, A. V. *Angew. Chem., Int. Ed.* **2011**, *50* (10), 2371.
- (35) Zaikina, J. V.; Mori, T.; Kovnir, K.; Teschner, D.; Senyshyn, A.; Schwarz, U.; Grin, Yu.; Shevelkov, A. V. *Chem. Eur. J.* **2010**, *16*, 12582.
- (36) Shevelkov, A. V.; Kovnir, K. *Struct. Bonding (Berlin)* **2011**, *139*, 97–142.
- (37) Shevelkov, A. V. *Usp. Khim.* **2008**, *77* (1), 3.
- (38) Um, T. Y.; Abe, T.; Sumi, S. *J. Mater. Synth. Proc.* **1999**, *7* (5), 303.
- (39) *STOE WinXPOW, Version 1.2*; STOE & Cie, Hilpertstr. 10, D-64295 Darmstadt, Germany, 2001.
- (40) Knapp, M.; Baetz, C.; Ehrenberg, H.; Fuess, H. *J. Synchrotron Radiat.* **2004**, *11*, 328.
- (41) Knapp, M.; Joco, V.; Baetz, C.; Brecht, H. H.; Berghaeuser, A.; Ehrenberg, H.; von Seggern, H.; Fuess, H. *Nucl. Instrum. Methods Phys. Res.* **2004**, *521* (2 – 3), 565.
- (42) Akselrud, L. G.; Zavalij, P. Y.; Grin, Yu.; Pecharsky, V. K.; Baumgartner, B.; Wölfel, E. *Mater. Sci. Forum.* **1993**, *335*, 133.
- (43) Sheldrick, G. M. *Acta Crystallogr., Sect. A* **2008**, *64*, 112.
- (44) Blessing, R. H. *Acta Crystallogr., Sect. A* **1995**, *51*, 33.
- (45) Emsley, J. *The Elements*; Clarendon Press: Oxford, U.K., 1991.
- (46) Kishimoto, K.; Akai, K.; Muraoka, N.; Koyanagi, T.; Matsuura, M. *Appl. Phys. Lett.* **2006**, *89* (17), 172106.
- (47) Sales, B. C.; Mandrus, D. G.; Chakoumakos, B. C. *Recent Trends in Thermoelectric Materials Research II*; Academic Press: New York, 2001; Vol. 70, pp 1–36.
- (48) Sales, B. C.; Chakoumakos, B. C.; Mandrus, D.; Sharp, J. W. *J. Solid State Chem.* **1999**, *146* (2), 528.
- (49) Christensen, M.; Lock, N.; Overgaard, J.; Iversen, B. B. *J. Am. Chem. Soc.* **2006**, *128*, 15657.
- (50) Christensen, M.; Iversen, B. B. *Chem. Mater.* **2007**, *19*, 4896.
- (51) Yan, X.; Grytsiv, A.; Giester, G.; Bauer, E.; Rogl, P.; Paschen, S. *J. Electron. Mater.* **2011**, *40* (5), 589.
- (52) Tanaka, T.; Onimaru, T.; Suekuni, K.; Mano, S.; Fukuoka, H.; Yamanaka, S.; Takabatake, T. *Phys. Rev. B* **2010**, *81*, 165110.
- (53) Kaltzoglou, A.; Fassler, T.; Christensen, M.; Johnsen, S.; Iversen, B.; Presniakov, I.; Sobolev, A.; Shevelkov, A. *J. Mater. Chem.* **2008**, *18*, 5630.
- (54) Nolas, G. S.; Ward, J. M.; Gryko, J.; Qiu, L.; White, M. A. *Phys. Rev. B* **2001**, *64* (15), 153201.
- (55) Okada, Y.; Tokumaru, Y. *J. Appl. Phys.* **1984**, *56* (2), 314.
- (56) Falmbigl, M.; Rogl, G.; Rogl, P.; Kriegisch, M.; Müller, H.; Bauer, E.; Reinecker, M. *J. Appl. Phys.* **2010**, *108*, 043529.
- (57) Kaibe, H.; Tanaka, Y.; Sakata, M.; Nishida, I. *J. Phys. Chem. Solids* **1989**, *50* (9), 945.
- (58) Zeller, R. C.; Pohl, R. O. *Phys. Rev. B* **1971**, *4* (6), 2029.
- (59) Slack, G. A. In *CRC Handbook of Thermoelectrics*; Rowe, D. M., Ed.; CRC Press: Boca Raton, FL, 1995.